CrystEngComm

PAPER

View Article Online
View Journal | View Issue

Cite this: *CrystEngComm*, 2024, **26**, 5099

Designed synthesis of Co(II) coordination polymers for evaluation of structural transformations†

Chia-Yi Lee,[a] Muhammad Usman,[a] Song-Wei Wang,[a] Kedar Bahadur Thapa,[b] Tsun-Ren Chen*[c] and Jhy-Der Chen *[a]

Received 20th July 2024,
Accepted 13th August 2024

DOI: 10.1039/d4ce00723a

rsc.li/crystengcomm

Five coordination polymers constructed from Co(II) salts, *N*,*N*′-bis(3-pyridylmethyl)oxalamide (**L**) and 4,4′-methylenedibenzoic acid (H_2MBA), {[Co(**L**)(MBA)(H_2O)]·H_2O}$_n$, **1**, {[Co(**L**)(MBA)]·4H_2O}$_n$, **2**, {[Co(**L**)(MBA)]·0.25H_2O}$_n$, **3**, [Co(**L**)(MBA)(H_2O)$_2$]$_n$, **4**, and {[Co(**L**)$_{0.5}$(MBA)(H_2O)$_2$]·CH_3OH}$_n$, **5**, are reported, which have been structurally characterized by using single crystal X-ray crystallography. Complexes **1** and **4** have the same formula, but differ in the number of coordinated and cocrystallized water molecules, whereas **2** and **3** form a pair of supramolecular isomers with different numbers of cocrystallized water molecules. Complexes **1** and **4** show interdigitated 2D layers with a (6^4·8·10)(6)-2,4L3 topology, which differ in the ligand conformations of **L** and bonding modes of MBA^{2-}. Complex **2** shows 2-fold interpenetrated 2D layers with a (6^4·8·10)(6)-2,4L3 topology and **3** displays a 2-fold interpenetrated 3D framework with a (4·6^2)(4·6^6·8^3)-**fet** topology, whereas **5** is a 1D ladder with a (6^2·10)(6)-2,3C1 topology, indicating that the coordination and/or cocrystallization of solvent molecules are important in determining their structural diversity. The structural transformations of **1**–**4** are also evaluated.

Introduction

Coordination polymers (CPs) with intriguing structural diversity and properties have been intensively investigated due to their potential applications in sensing, selective adsorption, gas storage, heterogeneous catalysis, magnetism, and luminescence.[1–11] The structural diversity of CPs thus prepared is governed by the identity of the metal ion, and the length, softness, coordination ability and donor-atom direction of the ligands as well as the reaction conditions such as the solvent system, temperature and time. On the other hand, structural transformations of CPs, which can be initiated by the removal and exchange of cocrystallized solvent or exposure to reactive vapors and external stimuli such as heat, light, and mechanical energy, are important phenomena for application in switches and sensors.[12–17]

Although diverse structures can be observed for CPs, those showing structural transformation are hardly expected. Great effort remains necessary to enlighten the factors that may direct the structural diversity and structural transformations. Structural transformations have been observed in several bis-pyridyl-bis-amide (bpba)-based CPs supported by polycarboxylate ligands,[18–24] demonstrating that the flexible nature of the bpba ligands and the various bonding modes of the polycarboxylate anions play important roles in promoting the reversible and irreversible structural transformations therein. Moreover, it is essential to prepare diverse CPs containing the same metal ion and organic ligand to investigate the structural transformations of CPs. Therefore, designed synthesis of the target products by careful evaluation of the metal to ligand ratio and reaction conditions is attempted.

Herein, we report the synthesis and structural characterization of five new CPs constructed from Co(II) salt, *N*,*N*′-bis(3-pyridylmethyl)oxalamide (**L**), Fig. 1, and 4,4′-methylenedibenzoic acid (H_2MBA), {[Co(**L**)(MBA)

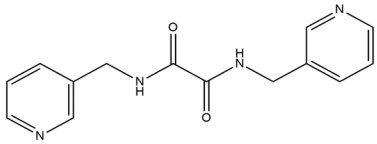

Fig. 1 Structure of *N*,*N*′-bis(3-pyridylmethyl)oxalamide (**L**).

[a] *Department of Chemistry, Chung Yuan Christian University, Chung-Li 320, Taiwan, Republic of China. E-mail: jdchen@cycu.edu.tw*
[b] *Makawanpur Multiple Campus, Affiliated to Tribhuvan University, Municipality Rd, Hetauda, Nepal*
[c] *Department of Applied Chemistry, National Pingtung University, Pingtung 90003, Taiwan, Republic of China. E-mail: trchen@mail.nptu.edu.tw*

† Electronic supplementary information (ESI) available: IR spectra (Fig. S1, S2 and S22). Yields (Table S1). PXRD patterns (Fig. S3–S7 and Fig. S13– S21). TGA curves (Fig. S8–S12). Elemental analysis (Fig. S23). CCDC no. 2369132–2369136 contain the supplementary crystallographic data for this paper. For ESI and crystallographic data in CIF or other electronic format see DOI: https://doi.org/10.1039/d4ce00723a

$(H_2O)]\cdot H_2O\}_n$, **1**, $\{[Co(L)(MBA)]\cdot 4H_2O\}_n$, **2**, $\{[Co(L)(MBA)]\cdot 0.25H_2O\}_n$, **3**, $[Co(L)(MBA)(H_2O)_2]_n$, **4**, and $\{[Co(L)_{0.5}(MBA)(H_2O)_2]\cdot CH_3OH\}_n$, **5**. The factors that govern the structural diversity and structural transformation of these CPs are also illuminated.

Experimental details

General procedures

IR spectra (KBr disk) were obtained on a JASCO FT/IR-460 plus spectrometer. Elemental analyses were performed using an Elementar Vario EL III or an Elementar Vario EL cube type analyzer. Thermal gravimetric analysis (TGA) measurements were carried out on a SII Nano Technology Inc. TG/DTA 6200 over the temperature range of 30 to 900 °C at a heating rate of 10 °C min^{-1} under N_2. Powder X-ray diffraction patterns were measured by using a Bruker D2 PHASER diffractometer with CuK_α (λ_α = 1.54 Å) radiation.

Materials

The reagent $Co(OAc)_2\cdot 4H_2O$ was purchased from J. T. Baker Co., and H_2MBA from Matrix Scientific Co. The ligand *N*,*N*′-bis(3-pyridylmethyl)oxalamide (**L**) was prepared according to a published procedure.[25]

Preparation of $\{[Co(L)(MBA)(H_2O)]\cdot H_2O\}_n$, 1. A mixture of $Co(OAc)_2\cdot 4H_2O$ (0.050 g, 0.20 mmol), **L** (0.027 g, 0.10 mmol) and H_2MBA (0.026 g, 0.10 mmol) was placed in a 23 mL Teflon reaction flask containing 8 mL H_2O and 2 mL MeOH, which was sealed and heated at 80 °C for 96 h under autogenous pressure and then the reaction system was cooled to room temperature at a rate of 2 °C per hour. Violet crystals suitable for single-crystal X-ray diffraction were obtained. Yield: 0.025 g (20%). Anal. calcd for $C_{29}H_{28}CoN_4O_8$ (M_W = 619.48): C, 56.21; H, 4.56; N, 9.05%. Found: C, 55.79; H, 4.40; N, 8.88%. FT-IR (cm^{-1}): 3505 (m), 3225 (w), 3043 (w), 1657 (s), 1607 (s), 1513 (s), 1430 (m), 1392 (m), 1355 (m), 1034 (m), Fig. S1.†

Preparation of $\{[Co(L)(MBA)]\cdot 4H_2O\}_n$, 2. Complex **2** was prepared by following the similar procedures for **1**, except that a mixture of $Co(OAc)_2\cdot 4H_2O$ (0.050 g, 0.20 mmol), **L** (0.027 g, 0.10 mmol) and H_2MBA (0.026 g, 0.10 mmol) in 5 mL H_2O and 5 mL MeOH was heated at 60 °C for 24 h. Dark purple crystals were obtained. Yield: 0.030 g (23%). Anal. calcd for $C_{29}H_{32}CoN_4O_{10}$ (M_W = 655.51): C, 53.12; H, 4.92; N, 8.55%. Found: C, 53.18; H, 4.54; N, 8.84%. FT-IR (cm^{-1}): 3503.54 (m), 3222.47 (w), 3043.60 (w), 1658.96 (s), 1631.48 (m), 1607.38 (s), 1512.40 (s), 1430.92 (w), 1397.17 (w), 1359.09 (w), 1034.62 (m), Fig. S1.†

Preparation of $\{[Co(L)(MBA)]\cdot 0.25H_2O\}_n$, 3. Complex **3** was prepared by following the similar procedures for **1**, except that a mixture of $Co(OAc)_2\cdot 4H_2O$ (0.050 g, 0.20 mmol), **L** (0.027 g, 0.10 mmol) and H_2MBA (0.026 g, 0.10 mmol) in 10 mL H_2O was heated at 120 °C for 48 h. Light purple crystals were obtained. Yield: 0.027 g (23%). Anal. calcd for $C_{29}H_{24.5}CoN_4O_{6.25}$ (M_W = 587.95): C, 59.22; H, 4.20; N, 9.53%. Found: C, 59.30; H, 3.94; N, 9.40%. FT-IR (cm^{-1}): 3503 (w), 3349 (w), 3259 (w), 1657 (m), 1596 (s), 1513 (m), 1430 (w), 1384 (w), 1351 (m), 1034 (m), Fig. S1.†

Preparation of $[Co(L)(MBA)(H_2O)_2]_n$, 4. Complex **4** was prepared by following the similar procedures for **1**, except that a mixture of $Co(OAc)_2\cdot 4H_2O$ (0.050 g, 0.20 mmol), **L** (0.027 g, 0.10 mmol) and H_2MBA (0.026 g, 0.10 mmol) in 10 mL H_2O was heated at 80 °C for 48 h. Light pink crystals were obtained. Yield: 0.026 g (21%). Anal. calcd for $C_{29}H_{28}CoN_4O_8$ (M_W = 619.12): C, 56.21; H, 4.56; N, 9.05%. Found: C, 56.05; H, 4.43; N, 9.31%. FT-IR (cm^{-1}): 3503 (m), 3239 (w), 3238 (w), 1657 (s), 1598 (s), 1514 (m), 1481 (w), 1391 (m), 1352 (w), 1035 (m), Fig. S1.†

Preparation of $\{[Co(L)_{0.5}(MBA)(H_2O)_2]\cdot CH_3OH\}_n$, 5. Complex **5** was prepared by following the similar procedures for **1**, except that a mixture of $Co(OAc)_2\cdot 4H_2O$ (0.050 g, 0.20 mmol), **L** (0.027 g, 0.10 mmol) and H_2MBA (0.06 g, 0.10 mmol) in 5 mL H_2O and 5 mL MeOH was heated at 60 °C for 96 h. Violet crystals were obtained. Yield: 0.017 g (16%). Anal. calcd for $C_{23}H_{25}CoN_2O_8$ (M_W = 516.38): C, 53.50; H, 4.88; N, 5.42%. Found: C, 53.75; H, 4.45; N, 6.29%. FT-IR (cm^{-1}): 3491 (w), 3397 (w), 3266 (w), 1683 (m), 1595 (s), 1545 (m), 1508 (w), 1435 (m), 1387 (s), 1190 (m), 1027 (s), Fig. S2.†

While the above-mentioned procedures afforded the major products **1–5**, some minor products can also be obtained, Table S1.†

X-ray crystallography

The diffraction data for complexes **1–5** were collected on a Bruker AXS SMART APEX II CCD diffractometer or Bruker D8 QUEST PHOTON III CPAD at 296 K, which was equipped with a graphite-monochromated Mo K_α (λ_α = 0.71073 Å) radiation source. Data reduction was performed by using standard methods and well-established computational procedures.[26] The structure factors were obtained after Lorentz and polarization corrections. An empirical absorption correction based on "multi-scan" was applied to the data for all complexes. The positions of some of the heavier atoms were located by the direct method. The remaining atoms were found in a series of alternating difference Fourier maps and least-squares refinements, while the hydrogen atoms except those of the water molecules were added by using the HADD command in SHELXTL 6.1012.[27] Table 1 lists the crystal data for complexes **1–5**.

Results and discussion

Synthesis of complexes 1–5

By careful evaluation of the metal to ligand ratio and reaction conditions, five distinct CPs constructed from Co(II) salts, **L** and H_2MBA can be achieved. Table S1† lists the reaction conditions and yields of each attempt, indicating that the yields of these complexes are dependent on the reaction time, temperature and solvent. While crystals of complexes **3**, **4** and **5** can be isolated directly from the reaction mixtures by the manipulation of the reaction temperatures, those of **1**

Table 1 Crystallographic data for complexes **1**–**5**

Complex	**1**	**2**	**3**	**4**	**5**
Formula	$C_{29}H_{28}CoN_4O_8$	$C_{29}H_{32}CoN_4O_{10}$	$C_{29}H_{24.5}CoN_4O_{6.25}$	$C_{29}H_{28}CoN_4O_8$	$C_{23}H_{25}CoN_2O_8$
Formula weight	619.48	655.51	587.95	619.48	516.38
Crystal system	Triclinic	Monoclinic	Monoclinic	Monoclinic	Triclinic
Space group	$P\bar{1}$	Pc	$P2_1/n$	$C2/c$	$P\bar{1}$
a, Å	10.1343(9)	8.9391(9)	11.4825(4)	27.7041(11)	9.834(4)
b, Å	10.7473(9)	9.8609(10)	21.8344(6)	9.3364(4)	11.041(5)
c, Å	13.9008(12)	17.5100(18)	11.8159(4)	10.6200(4)	11.166(5)
α, °	71.026(2)	90	90	90	85.008(10)
β, °	88.874(2)	93.993(2)	114.8619(9)	95.3715(13)	76.029(11)
γ, °	82.993(2)	90	90	90	85.758(11)
V, Å^3	1420.7(2)	1539.7(3)	2687.86(15)	2734.87(19)	1170.3(9)
Z	2	2	4	4	2
D_{calc}, Mg m^{-3}	1.448	1.414	1.453	1.505	1.465
$F(000)$	642	682	1214	1284	536
μ(Mo K$_\alpha$), mm^{-1}	0.662	0.619	0.691	0.687	0.784
Range (2θ) for data collection, °	$3.09 \le 2\theta \le 56.90$	$4.13 \le 2\theta \le 52.00$	$3.73 \le 2\theta \le 56.81$	$2.95 \le 2\theta \le 56.55$	$3.70 \le 2\theta \le 52.00$
Independent reflections	7105 [R(int) = 0.0652]	5787 [R(int) = 0.0529]	6710 [R(int) = 0.0486]	3382 [R(int) = 0.0512]	4604 [R(int) = 0.0718]
Data/restraints/parameters	7105/0/379	5787/2/397	6710/0/370	3382/0/200	4604/0/307
Quality-of-fit indicator[c]	1.009	1.005	1.022	1.027	1.007
Final R indices	R_1 = 0.0511,	R_1 = 0.0515,	R_1 = 0.0461,	R_1 = 0.0343,	R_1 = 0.0446,
[$I > 2\sigma(I)$][a,b]	wR_2 = 0.0948	wR_2 = 0.0997	wR_2 = 0.1010	wR_2 = 0.0795	wR_2 = 0.0843
R indices (all data)	R_1 = 0.0914,	R_1 = 0.0942,	R_1 = 0.0731,	R_1 = 0.0575,	R_1 = 0.0815,
	wR_2 = 0.1083	wR_2 = 0.1134	wR_2 = 0.1126	wR_2 = 0.0895	wR_2 = 0.0953

[a] $R_1 = \sum||F_o| - |F_c||/\sum|F_o|$. [b] $wR_2 = [\sum w(F_o^2 - F_c^2)^2/\sum w(F_o^2)^2]^{1/2}$. $w = 1/[\sigma^2(F_o^2 + (ap)^2 + (bp)]$, $p = [\max(F_o^2 \text{ or } 0) + 2(F_c^2)]/3$. $a = 0.03694$, $b = 0.4742$ for **1**; $a = 0.0467$, $b = 0$ for **2**; $a = 0.0425$, $b = 1.926$ for **3**; $a = 0.0425$, $b = 1.6437$ for **4**; $a = 0.0380$, $b = 0$ for **5**. [c] Quality-of-fit = $[\sum w(|F_o^2| - |F_c^2|)^2/(N_{observed} - N_{parameters})]^{1/2}$.

and **2** were obtained by manual separation based on the shapes and colours of the crystals.

Crystal structure of 1. Crystals of **1** conform to the triclinic space group $P\bar{1}$ and each asymmetric unit consists of one Co(II) ion, one **L** ligand, one MBA^{2-} ligand, one coordinated water molecule and one cocrystallized water molecule. Fig. 2(a) shows the coordination environment about the Co(II) metal center, which is six-coordinated by two nitrogen atoms from two **L** ligands [Co–N = 2.114(2) and 2.136(2) Å], three oxygen atoms from two MBA^{2-} ligands [Co–O = 2.0652(17)–2.2381(17) Å] and one oxygen atom from coordination water [Co–O = 2.1188(17) Å]. The Co(II) central metal atoms are bridged by MBA^{2-} and **L** to form a 2D layer. Topologically, if the Co(II) atoms are regarded as 4-connected nodes and the MBA^{2-} ligands as 2-connected nodes, whereas the **L** ligands are considered as linkers, the structure of **1** can be simplified as a 2,4-connected 2D net with a $(6^4{\cdot}8{\cdot}10)(6)$-2,4L3 topology, Fig. 2(b). Fig. 2(c) shows a pair of the 2D layers that are interdigitated to each other. On the other hand, if the MBA^{2-} ligands are also considered as linkers, the structure of **1** can be further simplified as a 2D net with a $(4^4{\cdot}6^2)$-**sql** topology.[28]

Crystal structure of 2. Crystals of **2** conform to the monoclinic space group Pc and each asymmetric unit consists of one Co(II) ion, one **L** ligand, one MBA^{2-} ligand and four cocrystallized water molecules. Fig. 3(a) shows the coordination environment about the Co(II) metal center, which is six-coordinated by two nitrogen atoms from two **L** ligands [Co–N = 2.082(5) and 2.086(6) Å] and four oxygen atoms from two MBA^{2-} ligands [Co–O = 2.047(5)–2.285(5) Å]. The Co(II) central metal atoms are bridged by MBA^{2-} and **L** to form a 2D layer. Topologically, if the Co(II) atoms are regarded as 4-connected nodes and the MBA^{2-} ligands as 2-connected nodes, whereas the **L** ligands are considered as linkers, the structure of **2** can be simplified as a 2,4-connected 2D net with a $(6^4{\cdot}8{\cdot}10)(6)$-2,4L3 topology, Fig. 3(b), showing a 2-fold interpenetration, Fig. 3(c). On the other hand, if the MBA^{2-} ligands are also considered as linkers, the structure of **2** can be further simplified as a 2-fold interpenetrated 2D net with a $(4^4{\cdot}6^2)$-**sql** topology.

Crystal structure of 3. Crystals of **3** conform to the monoclinic space group $P2_1/n$ and each asymmetric unit consists of one Co(II) ion, one **L** ligand, one MBA^{2-} ligand and a quarter of a cocrystallized water molecule. Fig. 4(a) shows the coordination environment about the Co(II) metal center, which is six-coordinated by two nitrogen atoms from two **L** ligands [Co–N = 2.152(2) and 2.165(2) Å] and four oxygen atoms from three MBA^{2-} ligands [Co–O = 1.9995(17)–2.2228(17) Å]. The Co(II) central metal atoms are bridged by MBA^{2-} to form dinuclear units, which are extended by **L** to form a 3D structure. Topologically, if the Co(II) atoms are regarded as 5-connected nodes and the MBA^{2-} ligands as 3-connected nodes, whereas the **L** ligands are considered as linkers, the structure of **3** can be simplified as a 3,5-connected net with a $(4{\cdot}6^2)(4{\cdot}6^6{\cdot}8^3)$-**fet** topology (standard representation), Fig. 4(b), showing a 2-fold interpenetration, Fig. 4(c). If the Co(II) dinuclear units are regarded as 6-connected nodes, while the organic ligands are considered as linkers, the structure of **3** can be simplified as a 6-connected net with a $\{4^{12}{\cdot}6^3\}$-**pcu** topology (cluster representation), Fig. 4(d), showing a 2-fold interpenetration, Fig. 4(e).

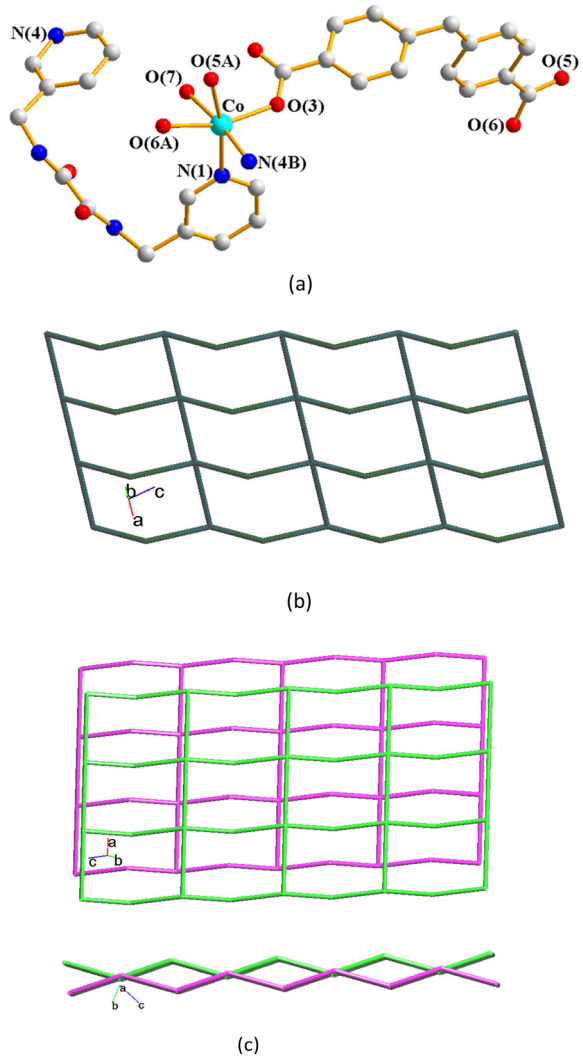

Fig. 2 (a) Coordination environment of the Co(II) ion in **1** showing the (6^4·8·10)(6)-2,4L3 topology. Symmetry transformations used to generate equivalent atoms: (A) *x*, *y* + 1, *z* − 1; (B) *x* − 1, *y*, *z*. (b) Topological structure of **1**, showing the (6^4·8·10)(6)-2,4L3 topology. (c) Two drawings showing a pair of interdigitated 2D layers in different directions.

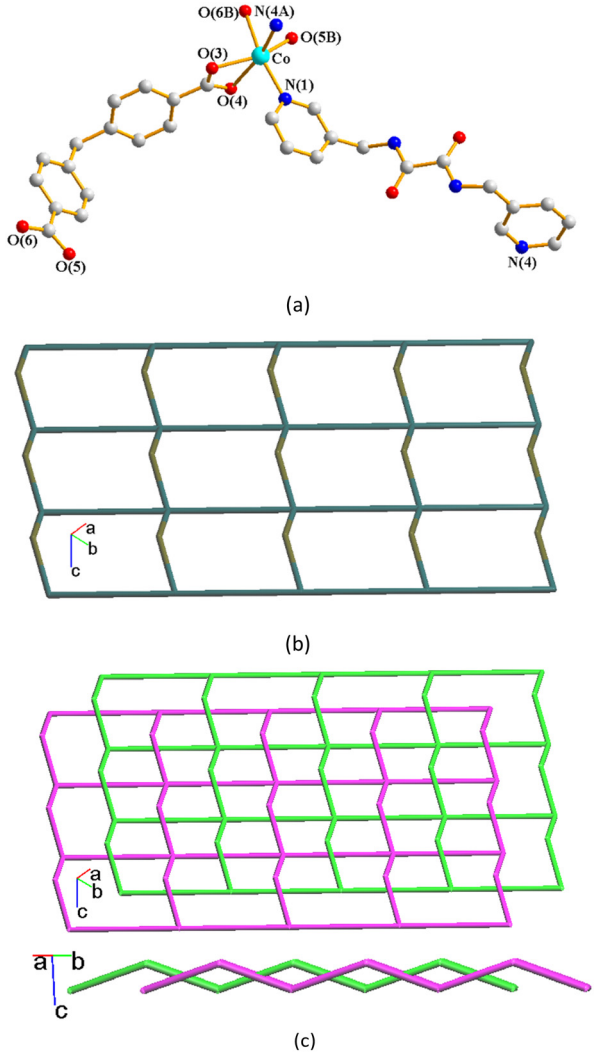

Fig. 3 (a) Coordination environment of the Co(II) ion in **2**. Symmetry transformations used to generate equivalent atoms: (A) *x* − 1, *y* − 1, *z*; (B) *x* − 1, *y* + 1, *z*. (b) Topological structure of **2**, showing the (6^4·8·10)(6)-2,4L3 topology. (c) Two drawings showing the 2-fold interpenetration in different directions.

Structure of 4. Crystals of **4** conform to the monoclinic space group *C*2/*c* and each asymmetric unit consists of one Co(II) ion, one **L** ligand, one MBA^{2-} ligand and two coordinated water molecules. Fig. 5(a) shows the coordination environment about the Co(II) metal center, which is six-coordinated by two nitrogen atoms from two **L** ligands, [Co–N = 2.2474(15) Å], two oxygen atoms from two MBA^{2-} ligands [Co–O = 2.0598(12)–2.0599(12) Å] and two oxygen atoms from coordination water [Co–O = 2.0890(14) Å]. The Co(II) central metal atoms are bridged by MBA^{2-} and **L** to form a 2D layer. Topologically, if the Co(II) atoms are regarded as 4-connected nodes and the MBA^{2-} ligands as 2-connected nodes, whereas the **L** ligands are considered as linkers, the structure of **4** can be simplified as a 2,4-connected 2D net with a (6^4·8·10)(6)-2,4L3 topology, Fig. 5(b). Fig. 5(c) shows a pair of the 2D layers that are interdigitated to each other. If the MBA^{2-} ligands are considered as linkers, the structure of **4** can be further simplified as a 4-connected net with a $\{4^4 \cdot 6^2\}$-**sql** topology.

Although complexes **1** and **4** adopt the same (6^4·8·10)(6)-2,4L3 topology with some degree of interdigitation, they are different in the evenness of the planes due to the different ligand conformations of **L** and bonding modes of MBA^{2-}, *vide infra*.

Structure of 5. Crystals of **5** conform to the triclinic space group $P\bar{1}$ and each asymmetric unit consists of one Co(II) ion, half an **L** ligand, one MBA^{2-} ligand, two coordinated water molecules and one cocrystallized MeOH molecule. Fig. 6(a) shows the coordination environment about the Co(II) metal center, which is six-coordinated by one nitrogen atom from the **L** ligand, [Co–N = 2.168(2) Å], two oxygen atoms from two MBA^{2-} ligands [Co–O = 2.019(2) - 2.202(2) Å] and two oxygen atoms from coordination water molecules [Co–O = 2.073(2)–

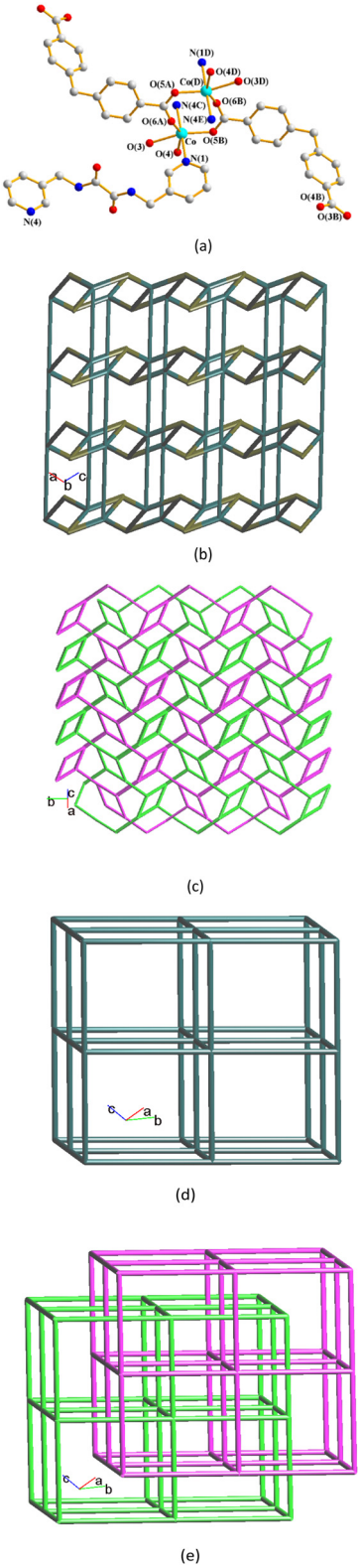

Fig. 4 (a) Coordination environment of the Co(II) ion in **3**. Symmetry transformations used to generate equivalent atoms: (A) $x - 1/2, -y + 3/2, z + 1/2$; (B) $-x + 5/2, y + 1/2, -z + 1/2$; (C) $x - 1, y, z - 1$; (D) $-x + 2, -y + 2, -z + 1$; (E) $-x + 3, -y + 2, -z + 2$. (b) Topological structure of **3**, showing a $(4{\cdot}6^2)(4{\cdot}6^6{\cdot}8^3)$-**fet** topology. (c) A drawing showing the 2-fold interpenetration with the **fet** topology. (d) Topological structure of **3**, showing the $\{4^{12}{\cdot}6^3\}$-**pcu** topology. (e) A drawing showing the 2-fold interpenetration with the **pcu** topology.

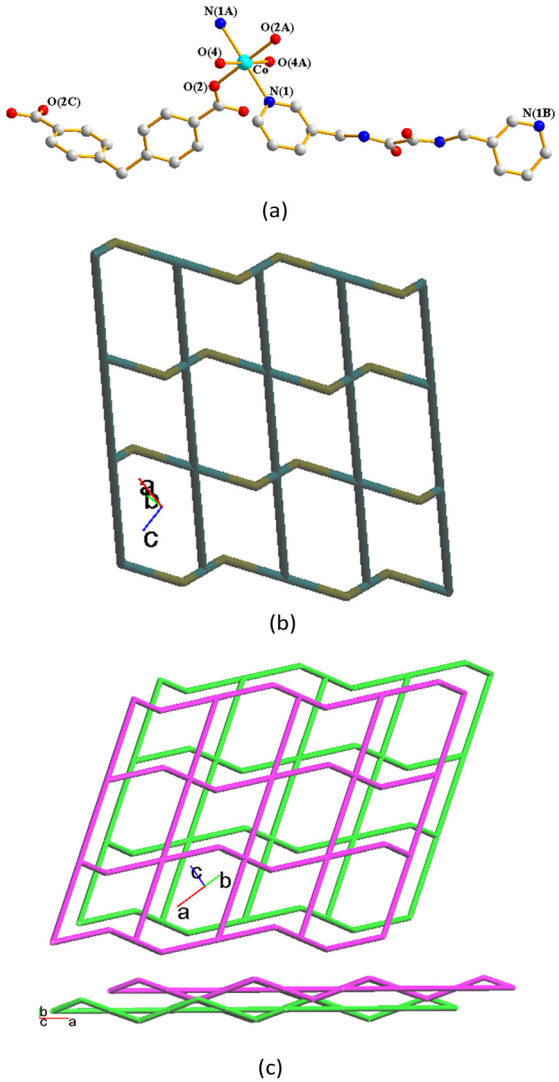

Fig. 5 (a) Coordination environment of the Co(II) ion in **4**. Symmetry transformations used to generate equivalent atoms: (A) $-x + 1/2, -y + 1/2, -z$; (B) $-x + 1, y, -z - 1/2$; (C) $-x, y, -z - 1/2$. (b) Topological structure of **4**, showing the $(6^4{\cdot}8{\cdot}10)(6)$-2,4L3 topology. (c) Two drawings showing a pair of interdigitated 2D layers in different directions.

2.105(2) Å]. The Co(II) central metal atoms are bridged by MBA^{2-} and **L** to form a 1D ladder. Topologically, if the Co(II) atoms are regarded as 3-connected nodes, and MBA^{2-} as 2-connected nodes, whereas the **L** ligands are considered as linkers, the structure of **5** can be simplified as a 2,3-connected 1D net with a $(6^2{\cdot}10)(6)$-2,3C1 topology, Fig. 6(b). If the MBA^{2-} ligands are also considered as linkers, the structure can be further simplified as a 3-connected net with a $(4^2{\cdot}6)$-$(4,4)(0,2)$ topology. Fig. 6(c).

Ligand conformations, bonding modes and structural types

For the ligand *N*,*N*′-bis(3-pyridylmethyl)oxalamide (**L**), the positions of the two C═O groups can be distinguished as *trans* or *cis*. When the two C═O groups show opposite

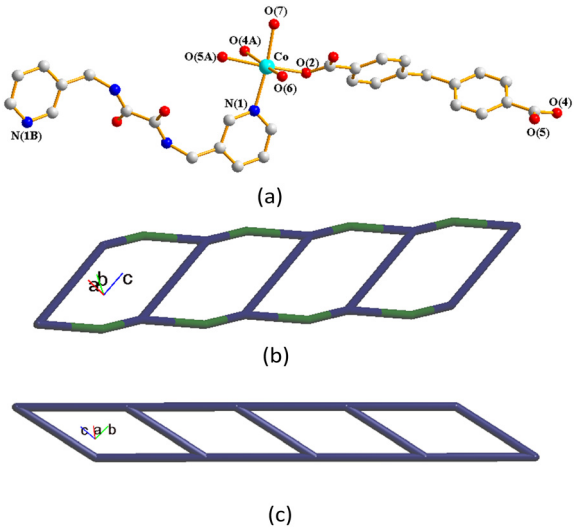

Fig. 6 (a) Coordination environment of the Co(II) ion in **5**. Symmetry transformations used to generate equivalent atoms: (A) $x, y + 1, z - 1$; (B) $-x + 1, -y + 2, -z$. (b) Topological structure of **5**, showing the $(6^2{\cdot}10)(6)$-2,3C1 topology. (c) Topological structure of **5**, showing the $(4^2{\cdot}6)$-(4,4)(0,2) topology.

directions, the position is defined as *trans*, and when they show the same direction, it is *cis*. Because of the different orientations adopted by the pyridyl nitrogen atoms and the amide oxygen atoms, three more conformations can be expressed as *anti–anti*, *syn–anti* and *syn–syn*. Accordingly, the ligand conformations of **L** in **1–5** are listed in Table 2, as well as the coordination modes of the MBA^{2-} ligands. Moreover, while the **L** ligands in **1–5** coordinate to the metal centers through the two pyridyl nitrogen atoms, the MBA^{2-} ligands bridge two or three metal atoms, showing μ_2-κ^2O,O′:κO″, μ_2-κ^2O,O′ κ^2O″,O‴, μ_3-κ^2O,O′:κO″:κO‴, μ_2-κO:κO′ and μ_2-κ^2O,O′:κO″ coordination modes, respectively, and resulting in 1-, 2- and 3D structures subject to the changes of the coordinated and cocrystallized solvent molecules. Complexes **2** and **3** can be regarded as a pair of supramolecular isomers[29] that cocrystallized with different numbers of water molecules, showing 2-fold interpenetrated 2D layers with a 2,4L3 topology and a 2-fold interpenetrated 3D framework with a **fet** topology, respectively.

Table 3 lists the CPs containing **L** that have been reported, demonstrating that the structural types of CPs based on **L** are governed by the polycarboxylate ligands and metal ions. Moreover, combination of **L** with 5-*tert*-IPA or MBA^{2-} may lead to the formation of entangled Co(II) CPs, revealing the importance of the identity of the supporting dicarboxylate ligands in the formation of the entangled CPs based on the semi-rigid **L**. In contrast, it is interesting to note that supported by the angular dicarboxylate ligand, the flexible bpba ligands may adopt the suitable conformations for the formation of the entangled Co(II) CPs.[30] Structural comparisons of **1–5** with four CPs derived from $Co(OAc)_2{\cdot}4H_2O$, **L** and 4,4′-

Table 2 Drawings showing the ligand conformations of **L** and the coordination modes of MBA^{2-} in **1–5**

	Ligand conformation	Coordination mode
1	*trans syn–syn*	μ_2-κ^2O,O′:κO″
2	*trans anti–anti*	μ_2-κ^2O,O′ κ^2O″,O‴
3	*trans syn–syn*	μ_3-κ^2O,O′:κO″:κO‴
4	*trans anti–syn*	μ_2-κO:κO′
5	*trans syn–syn*	μ_2-κ^2O,O′:κO″

sulfonyldibenzoic acid (H_2SDA), revealing non-entangled 2D layers with **sql**, 2,6L1, (4,4)Ia, and 6L12 topologies, respectively,[31] suggest that delicate change from the carbon atom to the SO_2 group that bridges the pyridyl rings of the angular dicarboxylate ligand drastically modifies the structural diversity. On the other hand, five Cd(II) CPs constructed from 1,4-bis(2-methyl-imidazol-1-yl) butane and 5-bromoisophthalic acid have been reported.[32]

Powder X-ray analysis and thermal properties

In order to check the bulk purity of the products, powder X-ray diffraction (PXRD) experiments have been carried out for all complexes. As shown in Fig. S3–S7,† the peak positions of the experimental and simulated PXRD patterns are in agreement with each other, which demonstrates that the crystal structures are truly representative of the bulk materials. The differences in intensity may be owing to the preferred orientation of the powder samples.

Thermal gravimetric analyses (TGA) were carried out to examine the thermal decomposition of all complexes, which were recorded from about 30 to 800 °C at 10 °C min^{-1} under a N_2 atmosphere, Fig. S8–S12.† Table 4 reveals that two-step decomposition involving loss of solvent molecules and loss of organic ligands is observed for all of the complexes.

Table 3 CPs based on L in mixed ligand systems

Complex	Structure	References
$\{[Ni(\mathbf{L})(OBA)(H_2O)]\cdot H_2O\}_n$	Interdigitated 2D, 2,4L2	25
$\{[Ni(\mathbf{L})(SDA)(H_2O)_2]\cdot H_2O\cdot CH_3OH\}_n$	2D, **sql**	25
$\{[Cd(\mathbf{L})(1,4\text{-NDC})(H_2O)]\cdot 5H_2O\}_n$	1D looped chain, 2,4C5	33
$\{[Co_2(\mathbf{L})_2(1,4\text{-NDC})_2(H_2O)_4]\cdot 3MeOH\cdot H_2O\}_n$	3D, **cds**	33
$[Zn(\mathbf{L})_{0.5}(FIPBB)\cdot H_2O]_n$	2D, **bey**	34
$[Co(\mathbf{L})(OBA)\cdot 2H_2O]_n$	2D, 3,5L2	34
$[Co(\mathbf{L})_{0.5}(FIPBB)]_n$	2D, **bey**	34
$[Co_2(\mathbf{L})_2(FIPBB)_2(H_2O)_5\cdot 4H_2O]_n$	1D looped chain, 2,2,2,4C10	34
$[Co(\mathbf{L})_{0.5}(1,2,4,5\text{-BTEC})_{0.5}(H_2O)]_n$	3D, 4,5,6T11	35
$\{[Co(\mathbf{L})(1,2,4,5\text{-BTEC})_{0.5}(H_2O)]\cdot H_2O\}_n$	2D, **bex**	35
$\{[Co(\mathbf{L})_{1.5}(1,2,4,5\text{-BTEC})_{0.5}(H_2O)]\cdot 3H_2O\}_n$	3D, **dmp**	35
$[Zn(\mathbf{L})_{0.5}(1,3,5\text{-HBTC})(H_2O)_2]_n$	1D looped chain	36
$\{[Cu(\mathbf{L})(1,3,5\text{-HBTC})]\cdot H_2O\}_n$	2D, **sql**	37
$\{[Co(\mathbf{L})(SDA)(H_2O)_2]\cdot H_2O\cdot CH_3OH\}_n$	2D, **sql**	31
$\{[Co(\mathbf{L})_{0.5}(SDA)]\cdot 2H_2O\cdot 0.5\mathbf{L}\}_n$	2D, 2,6L1	31
$\{[Co(\mathbf{L})_{1.5}(SDA)(H_2O)]\cdot H_2O\}_n$	2D, (4,4)Ia	31
$\{[Co_2(\mathbf{L})_{1.5}(SDA)_2(H_2O)_2]\cdot 4H_2O\}_n$	2D, 6L12	31
$\{[Co(\mathbf{L})(1,3,5\text{-HBTC})]\cdot H_2O\}_n$	2D, 3,5L2	35
$\{[Co(\mathbf{L})(5\text{-}tert\text{-IPA})(H_2O)_2]\cdot H_2O\}_n$	3-fold interpenetrated 2D, **hcb**	38
$[Co(\mathbf{L})_{0.5}(5\text{-}NH_2\text{-IPA})(H_2O)]_n$	2D, **bey**	38
$\{[Co(\mathbf{L})(MBA)(H_2O)]\cdot H_2O\}_n$	2D, 2,4L3	This work
$\{[Co(\mathbf{L})(MBA)]\cdot 4H_2O\}_n$	2-fold interpenetrated 2D, 2,4L3	This work
$\{[Co(\mathbf{L})(MBA)]\cdot 0.25H_2O\}_n$	2-fold interpenetrated 3D, **fet**	This work
$[Co(\mathbf{L})(MBA)(H_2O)_2]_n$	2D, 2,4L3	This work
$\{[Co(\mathbf{L})_{0.5}(MBA)(H_2O)_2]\cdot CH_3OH\}_n$	1D, 2,3C1	This work

Abbreviations: H_2OBA = 4,4-oxydibenzoic acid; H_2SDA = 4,4-sulfonyldibenzoic acid; 1,4-NDC = 1,4-naphthalenedicarboxylic acid; H_2FIPBB = 4,4′-hexafluoroisopropylidenebis(benzoic acid); 1,2,4,5-H_4BTEC = 1,2,4,5-bezenetetracarboxylic acid; 1,3,5-H_3BTC = 1,3,5-benzenetricarboxylic acid; 5-*tert*-H_2IPA = 5-*tert*-butylbenzene-1,3-dicarboxylic acid; 5-NH_2-H_2IPA = 5-aminoisophthalic acid.

Table 4 Thermal properties of complexes **1**–**5**

Complex	Weight loss of solvent °C (calc/found), %	Weight loss of ligand °C (calc/found), %
1	$2H_2O$ ~150 (5.80/7.19)	**L** + (MBA^{2-}) 200–800 (84.91/83.23)
2	$4H_2O$ ~200 (10.98/10.85)	**L** + (MBA^{2-}) 200–800 (80.24/79.82)
3	0.25 H_2O ~100 (0.77/0.31)	**L** + (MBA^{2-}) 250–800 (89.46/90.79)
4	$2H_2O$ ~200 (5.81/7.34)	**L** + (MBA^{2-}) 290–800 (84.90/85.46)
5	$2H_2O$ + MeOH ~130 (13.17/14.30)	0.5**L** + (MBA^{2-}) 250–800 (75.72/72.63)

Chemical stability and structural transformation of complexes 1–4

Complexes **1**–**4** provide a unique opportunity to study structural transformation due to the water removal and adsorption because they comprise the same metal center and organic ligand. We first checked their chemical stability in organic solvents. For each experiment, 10 mg of the complex was immersed in 10 mL of the solvent for a week, involving water, methanol (MeOH), ethanol (EtOH), ether, hexane, tetrahydrofuran (THF), acetonitrile (ACN), dichloromethane (DCM), dimethylacetamide (DMAC), and dimethylformamide (DMF), which was then filtered and then dried under vacuum. The PXRD patterns of these solid samples, Fig. S13–S16,† reveal that complexes **1**–**3** were not stable upon immersion in MeOH, DMF and water, respectively, whereas **4** retained its structure in all of the solvents.

The stabilities of complexes **1**–**4** upon removal of the cocrystallized/coordinated water molecules were then investigated. Complexes **1**–**4** were heated at 150, 200, 100 and 200 °C, respectively, for two hours to obtain fully desolvated samples, which were then immersed in various solvents. Fig. S17† shows the photos and PXRD patterns of complex **1**

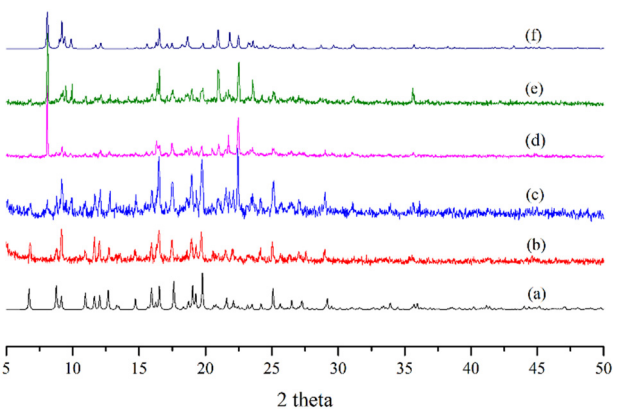

Fig. 7 PXRD patterns of (a) simulation of **1**, (b) as-synthesized **1**, (c) **1** heated at 150 °C for 2 h, (d) desolvated **1** in THF, (e) desolvated **1** in ACN and (f) simulation of **3**.

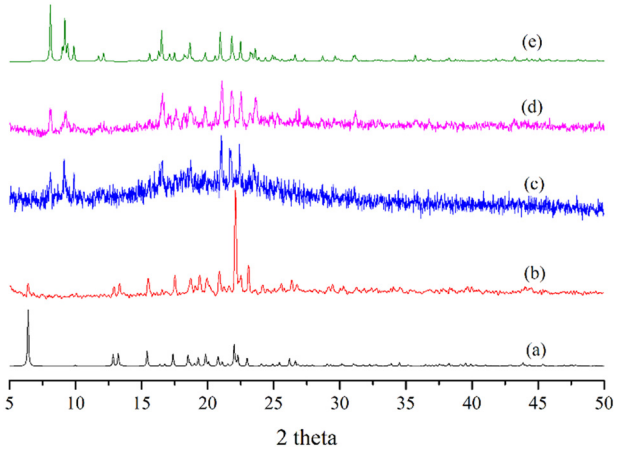

Fig. 8 PXRD patterns of (a) simulation of **4**, (b) as-synthesized **4**, (c) **4** heated at 200 °C for 2 h, (d) desolvated **4** in water and (e) simulation of **3**.

heated at 150 °C for 2 hours and then immersed in a variety of organic solvents, whereas Fig. 7 indicates that **1** is partially transformed into **3** upon desolvation and the desolvated sample can be effectively transformed into **3** in THF and ACN. Fig. S18 and S19† indicate that the framework of complex **2** decomposed upon desolvation and the desolvated sample of **3** retained its structure in the organic solvents. Moreover, Fig. S20† and 8 show that complex **4** can be transformed into **3** upon water removal, but the transformation is irreversible.

To check the possibility of structural transformation under hydrothermal conditions, complexes **1**–**4**, respectively, were heated in water at 120 °C for 2 days. Fig. S21† displays the PXRD patterns after the attempts, indicating that complexes **1**–**4** were all transformed into the same complex that was not structurally characterized by using single crystal X-ray diffraction. Supported by the IR spectra, Fig. S22,† and the elemental analysis, Fig. S23,† this unknown complex probably comprises only the Co(II) ion and MBA^{2-} ligand. Fig. 9 summarizes the synthetic pathways and structural transformations for complexes **1**–**4**.

Conclusions

The synthesis and structural characterization of five diverse Co(II) CPs comprising **L** and MBA^{2-} have been successfully accomplished. 1D, 2D and 3D structures can be shown for these CPs, demonstrating that cocrystallized and coordinated solvent molecules govern the structural diversity. The yields of these CPs were dependent on the metal-to-ligand ratio, solvent system, and reaction temperature. Modification of the bridging group of the angular dicarboxylate ligand from the SO_2 group[31] to the carbon atom has significantly altered the structural diversity of the Co(II) CPs thus prepared. Investigations on the chemical stability and structural transformation of **1**–**4** indicate that the desolvated sample of **1** can be transformed into **3** in THF and ACN, while **4** can be irreversibly transformed into **3** upon water removal. Designed synthesis of diverse CPs for the evaluation of structural transformations can thus be achieved if proper combination of the mixed ligands as well as adequate reaction conditions can be manipulated.

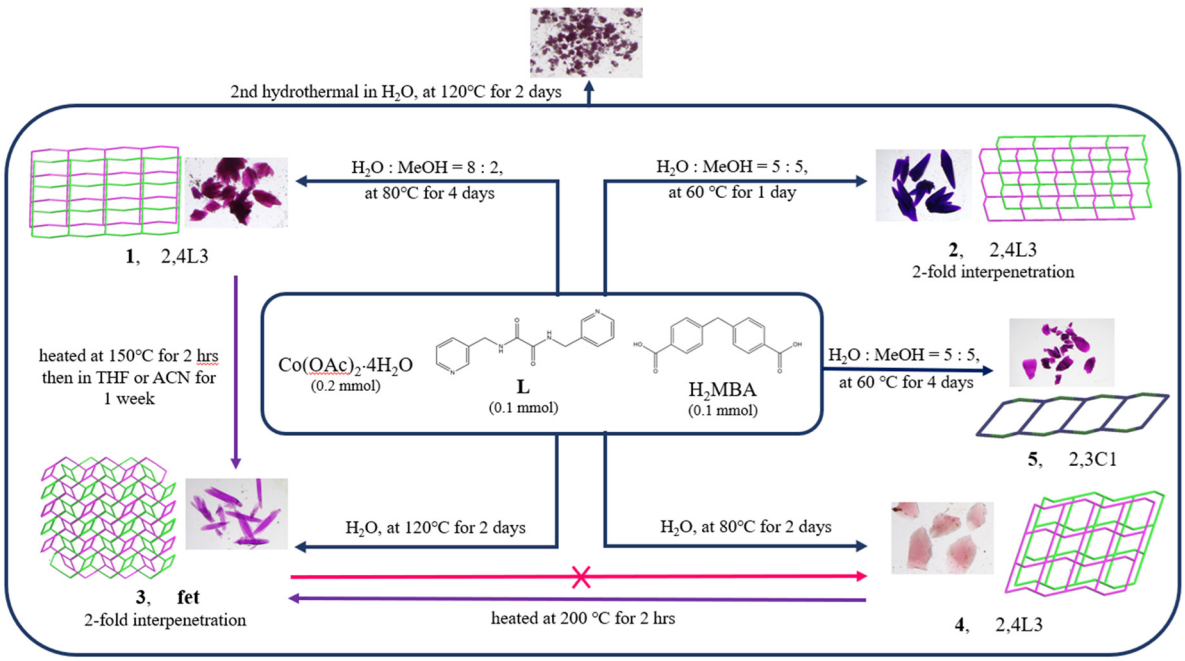

Fig. 9 Synthetic pathways and structural transformations for complexes **1**–**5**.

Data availability

The data supporting this article have been included as part of the ESI.† Crystallographic data for complexes **1**–**4** have been deposited at the CCDC with no. 2369132–2369136.

Author contributions

Investigation, C.-Y. L.; data curation, M. U., S.-W. W. and K. B. T.; review and supervision, T.-R. C. and J.-D. C. All authors have read and agreed to the published version of the manuscript.

Conflicts of interest

There are no conflicts to declare.

Acknowledgements

We are grateful to the National Science and Technology Council of the Republic of China for support.

References

1 S. R. Batten, N. R. Champness, X.-M. Chen, J. Garcia-Martinez, S. Kitagawa, L. Öhrstrom, M. O'Keeffe, M. P. Suh and J. Reedijk, *Pure Appl. Chem.*, 2013, **85**, 1715–1724.
2 D. J. Wales, J. Grand, V. P. Ting, R. D. Burke, K. J. Edler, C. R. Bowen, S. Mintova and A. D. Burrows, *Chem. Soc. Rev.*, 2015, **44**, 4290–4321.
3 E. R. T. Tiekink and J. J. Vittal, *Frontiers in Crystal Engineering*, John Wiley & Sons, Ltd., England, 2006.
4 M. Li, D. Li, M. O'Keeffe and O. M. Yaghi, *Chem. Rev.*, 2014, **114**, 1343–1370.
5 X.-K. Yang, W.-T. Lee, J.-H. Hu and J.-D. Chen, *CrystEngComm*, 2021, **23**, 4486–4493.
6 S. Mondal and P. Dastidar, *Cryst. Growth Des.*, 2020, **20**, 7411–7420.
7 S. R. Batten, S. M. Neville and D. R. Turner, *Coordination Polymers: Design, Analysis and Application*, Royal Society of Chemistry, Cambridge, UK, 2009.
8 Sh. Li, B. Wang, G. Liu, X. Li, C. Sun, Z. Zhang and X. Wang, *Inorg. Chem. Front.*, 2024, **11**, 1561–1572.
9 X.-D. Zhang, J.-A. Hua, J.-H. Guo, Y. Zhao and W.-Y. Sun, *J. Mater. Chem. C*, 2018, **6**, 12623–12630.
10 X. Wu, D. Li, L. Xu, Y.-F. Jiang, Y. Zhao and J. Zhao, *CrystEngComm*, 2023, **25**, 3222–3228.
11 Z.-P. Chen, D. Li, L. Xu, Y.-F. Jiang, K. Lin, Y. Zhao and J. Zhao, *New J. Chem.*, 2022, **46**, 12994–13000.
12 J. J. Vittal, *Coord. Chem. Rev.*, 2007, **251**, 1781–1795.
13 G. K. Kole and J. J. Vittal, *Chem. Soc. Rev.*, 2013, **42**, 1755–1775.
14 G. Chakraborty, I.-H. Park, R. Medishetty and J. J. Vittal, *Chem. Rev.*, 2021, **121**, 3751–3891.
15 D. Liu, Z.-G. Ren, H.-X. Li, J.-P. Lang, N.-Y. Li and B. F. Abrahams, *Angew. Chem., Int. Ed.*, 2010, **49**, 4767–4770.
16 F.-L. Hu, Y. Mi, C. Zhu, B. F. Abrahams, P. Braunstein and J.-P. Lang, *Angew. Chem., Int. Ed.*, 2018, **57**, 12696–12701.
17 M.-F. Wang, Y. Mi, F.-L. Hu, Z. Niu, X.-H. Yin, Q. Huang, H.-F. Wang and J.-P. Lang, *J. Am. Chem. Soc.*, 2020, **142**, 700–704.
18 C.-H. Hsu, W.-C. Huang, X.-K. Yang, C.-T. Yang, P. M. Chhetri and J.-D. Chen, *Cryst. Growth Des.*, 2019, **19**, 1728–1737.
19 X.-K. Yang and J.-D. Chen, *CrystEngComm*, 2019, **21**, 7437–7446.
20 Y.-F. Liu, J.-H. Hu, W.-T. Lee, X.-K. Yang and J.-D. Chen, *Cryst. Growth Des.*, 2020, **20**, 7211–7218.
21 C.-J. Chen, W.-T. Lee, J.-H. Hu, P. M. Chhetri and J.-D. Chen, *CrystEngComm*, 2020, **22**, 7565–7574.
22 C.-J. Chen, C.-L. Chen, W.-T. Lee, J.-H. Hu, P. M. Chhetri and J.-D. Chen, *J. Mol. Struct.*, 2021, **1244**, 131252.
23 J.-H. Hu, Y.-C. Liu and J.-D. Chen, *CrystEngComm*, 2021, **23**, 7471–7478.
24 J.-H. Hu, Y.-C. Liu, Y.-H. Liu and J.-D. Chen, *CrystEngComm*, 2022, **24**, 4120–4127.
25 W.-T. Lee, T.-T. Liao and J.-D. Chen, *Int. J. Mol. Sci.*, 2022, **23**, 3603.
26 *Bruker AXS, APEX2, V2008.6, SAD ABS V2008/1, SAINT+V7.60A, SHELXTL V6.14*, Bruker AXS Inc., Madison, Wisconsin, USA, 2008.
27 G. M. Sheldrick, *Acta Crystallogr., Sect. C: Struct. Chem.*, 2015, **71**, 3–8.
28 V. A. Blatov, A. P. Shevchenko and D. M. Proserpio, *Cryst. Growth Des.*, 2014, **14**, 3576–3586.
29 J.-P. Zhang, X.-C. Huang and X.-M. Chen, *Chem. Soc. Rev.*, 2009, **38**, 2385–2396.
30 W.-C. Huang, W.-H. Chen, C.-L. Chen, T.-T. Liao, Y.-W. Chen and J.-D. Chen, *CrystEngComm*, 2023, **25**, 5575–5587.
31 C.-Y. Lee, Y.-H. Ye, S.-W. Wang and J.-D. Chen, *Molecules*, 2024, **29**, 1748.
32 Y.-F. Hou, B. Liu, K.-F. Yue, C.-S. Zhou, Y.-M. Wang, N. Yan and Y.-Y. Wang, *CrystEngComm*, 2014, **16**, 9560–9567.
33 W.-J. Chen, C.-Y. Lee, Y.-H. Huang and J.-D. Chen, *Polyhedron*, 2022, **223**, 115991.
34 V. Lakshmanan, C.-Y. Lee, Y.-W. Tseng, Y.-H. Liu, C.-H. Lin and J.-D. Chen, *CrystEngComm*, 2022, **24**, 6076–6086.
35 T.-T. Liao, S.-Y. Lin and J.-D. Chen, *CrystEngComm*, 2023, **25**, 1723–1730.
36 J.-H. Hu, H.-H. Hsu, Y.-W. Chen, W.-H. Chen, S.-M. Liu and J.-D. Chen, *J. Mol. Struct.*, 2023, **1289**, 135896.
37 S.-Y. Lin, Y.-L. Shen and W.-H. Chen, *Molecules*, 2024, **29**, 311.
38 J.-H. Hu, Y.-H. Ye, Y.-W. Chen, S.-M. Liu and J.-D. Chen, *J. Mol. Struct.*, 2024, **1312**, 138544.